Joule

CellPress

Article

Design of Red Phosphorus Nanostructured Electrode for Fast-Charging Lithium-Ion Batteries with High Energy Density

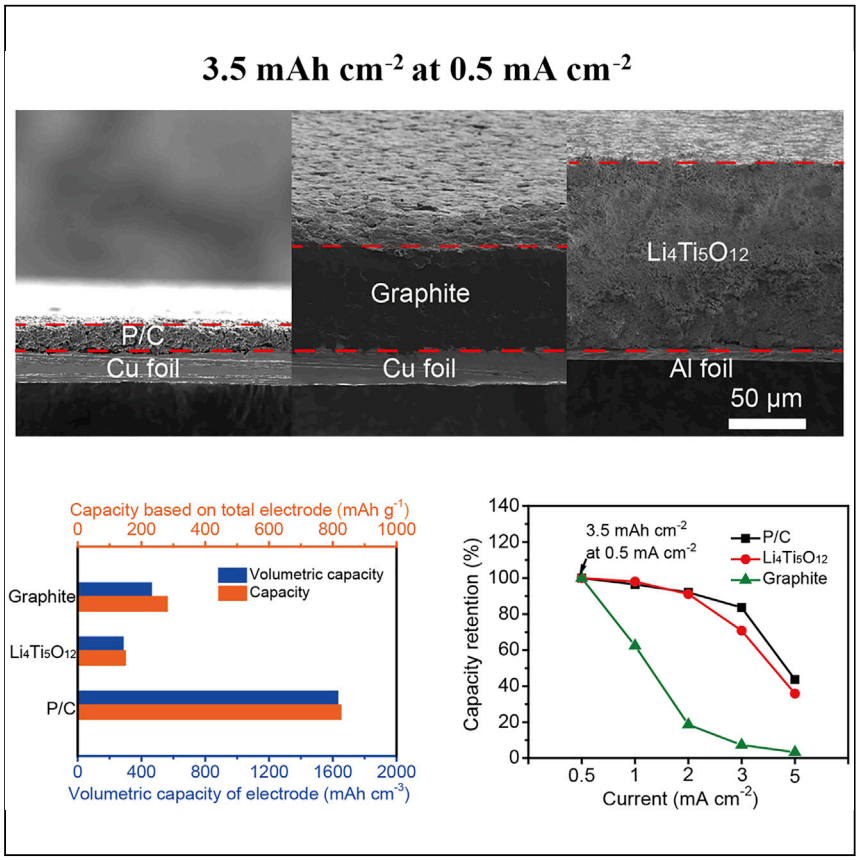

We propose red phosphorus (P) as an ideal anode for fast-charging lithium-ion batteries and demonstrate a red P-carbon nanocomposite with excellent fast-charging capability, high capacity based on the volume and weight of the whole electrode, and stable cycling with 100.0% (±0.1%) Coulombic efficiency at a high-areal-capacity loading, meeting the standards of industrial applications.

Yongming Sun, Li Wang, Yanbin Li, ..., Allen Pei, Xiangming He, Yi Cui

yicui@stanford.edu

HIGHLIGHTS

Important missing principles for fast-charging materials have been proposed

Red P/C electrode with good volume accommodation has been fabricated

The P anode delivers excellent fast-charging capability and high overall capacity

Sun et al., Joule 3, 1–14
April 17, 2019
https://doi.org/10.1016/j.joule.2019.01.017

Please cite this article in press as: Sun et al., Design of Red Phosphorus Nanostructured Electrode for Fast-Charging Lithium-Ion Batteries with High Energy Density, Joule (2019), https://doi.org/10.1016/j.joule.2019.01.017

Joule

CellPress

Article

Design of Red Phosphorus Nanostructured Electrode for Fast-Charging Lithium-Ion Batteries with High Energy Density

Yongming Sun,[1,2,6] Li Wang,[2,3,6] Yanbin Li,[2] Yuzhang Li,[2] Hye Ryoung Lee,[2] Allen Pei,[2] Xiangming He,[3] and Yi Cui[2,4,5,7,*]

SUMMARY

We propose that red phosphorus (P) is an ideal anode material for fast-charging lithium-ion batteries (LIBs) because of the combined advantages of high capacity (6,075 mAh cm^{-3}) and relatively low yet safe lithiation potential (~0.7 V versus Li/Li^+). A red P/C nanocomposite has been fabricated, featuring amorphous red P nanodomains embedded in the nanopores of micrometer-scale porous conductive carbon with interior nanoscale void spaces, a conductive P-free carbon superficial layer, and a high tap density of 1.0 g cm^{-3}. At an industrial-level areal capacity (3 mAh cm^{-2} or higher), a P/C electrode shows considerably better fast-charging capability than commercial graphite and $Li_4Ti_5O_{12}$ electrodes, as well as much higher volumetric capacity and specific capacity based on the whole electrode. Meanwhile, our P/C electrode shows excellent long-term cycling stability with Coulombic efficiency of 100.0% (±0.1%) and 90% capacity retention from the 5th to 500th cycles.

Context & Scale

We propose that red P is an attractive anode material for high-energy-density, fast-charging LIBs due to its high capacity and relatively low, yet safe, lithiation potential. We demonstrate that electrodes utilizing a red P/C nanocomposite with an optimized structure display much better rate capability and much higher overall capacity than that of the commercial graphite and $Li_4Ti_5O_{12}$ electrodes at the areal-capacity level of a commercial Li-ion battery cell.

INTRODUCTION

High-energy-density lithium (Li)-ion batteries (LIBs) with superior fast-charging capability are highly desirable for portable electronics and electric vehicles.[1–5] However, the energy and power density of LIBs based on the conventional intercalation-type graphite anode and the $LiCoO_2$ cathode are approaching their theoretical limit.[6,7] Recently, extensive research has been conducted with a focus on increasing the energy density of Li-based batteries by using new battery chemistries, such as silicon (Si)[8–10] and Li metal[11,12] anodes, sulfur (S) (Li-S batteries),[13–16] and oxygen (O_2) (Li-air batteries)[17–19] cathodes, while less attention has been paid to improving the charging rate capability of batteries.

Low ionic and electronic conductivities of materials lead to sluggish solid-state diffusion processes and have long been considered the main reasons for the inferior rate capability of electrodes and the low power density of LIBs.[20] The most common strategies to address these challenges are to use nanoscale particles and conducting coatings, which reduce the ion and electron transport distance and improve conductivity at the particle level. Successful examples using such strategies have been shown for traditional intercalation-type electrode materials (e.g., $Li_4Ti_5O_{12}$[21,22] and $LiFePO_4$[23]). Very recently, a three-dimensional holey graphene-Nb_2O_5 composite was designed and delivered excellent rate capability because of its good charge carrier transport properties.[24] Moreover, carbon-coated Li_3VO_4 spheres have been successfully synthesized and showed great advances as high-rate anode materials.[25] However, when the areal capacity of these electrodes reaches substantially high

Please cite this article in press as: Sun et al., Design of Red Phosphorus Nanostructured Electrode for Fast-Charging Lithium-Ion Batteries with High Energy Density, Joule (2019), https://doi.org/10.1016/j.joule.2019.01.017

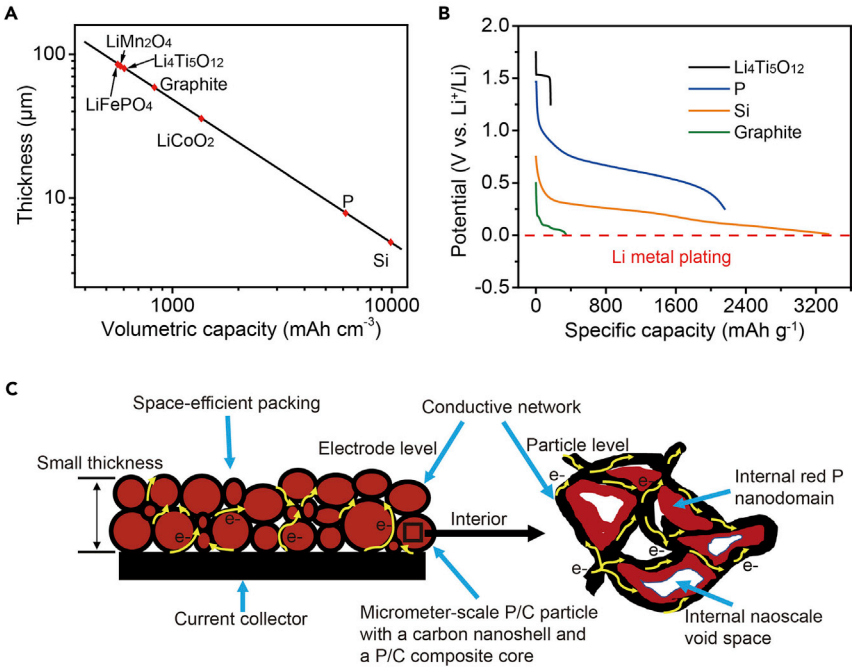

Figure 1. Schematic of Material Choice and Structure for Fast-Charging LIBs

(A) Calculated thicknesses of the electrodes versus theoretical volumetric capacities of materials. The calculation is based on electrodes with an areal capacity of 3.5 mAh cm^{-2}, 20% porosity, 90% active material volume percentage, and theoretical volumetric capacities of active materials.

(B) Lithiation potential curves for typical anodes ($Li_4Ti_5O_{12}$, graphite, red P, and Si). Red P is an ideal anode material for fast-charging LIBs due to the combined advantages of high capacity and reasonable lithiation potential: relatively low to achieve high-cell-output voltage, relatively high to realize high-capacity retention at high charging current densities with large overpotentials and avoid Li-metal plating without safety concerns.

(C) Structural design for P-based material and electrodes with good electronic conductivity, space-efficient packing, and good stability: micrometer-scale P/C composite grain with a conductive carbon superficial layer, a P/C composite core, internal nanoscale void space, and red P nanodomain.

levels (e.g., >3 mAh cm^{-2}), their rate capability is greatly reduced because of increasing charge carrier diffusion lengths in thicker electrodes. Also, the energy density of LIBs using these low-capacity materials is significantly limited due to the large volume and weight of electrodes.

To make a good electrode for LIBs with high energy and high power density, we believe that high capacity and suitable working potential of the electrode materials are two other important parameters in addition to good electronic and ionic conductivity. For a given electrode areal capacity, porosity, and active material volume percentage, the higher the volumetric capacity the material delivers, the smaller the thickness of the electrode is and the shorter the charge carrier transport paths are within the electrode (Figure 1A), leading to better rate performance. This reduction in volume and weight of the electrodes by using high-capacity battery materials also significantly increases the overall battery energy density. In parallel, suitable working potential is also of vital importance to realize LIBs that combine high energy and power density. In principle, the cathode potential should be high and the anode potential should be low to achieve a high cell output voltage and high energy density. However, to realize high capacity retention during fast charge, the intrinsic working potential of the cathode should be moderately low to buffer the large overpotentials and to prevent overshooting the cycling voltage cutoffs or electrolyte

[1]Wuhan National Laboratory for Optoelectronics and School of Optical and Electronic Information, Huazhong University of Science and Technology, Wuhan, Hubei 430074, P.R. China

[2]Department of Materials Science and Engineering, Stanford University, Stanford, CA 94305, USA

[3]Institute of Nuclear and New Energy Technology, Tsinghua University, Beijing 100084, P.R. China

[4]Stanford Institute for Materials and Energy Sciences, Stanford, CA 94025, USA

[5]SLAC National Accelerator Laboratory, 2575 Sand Hill Road, Menlo Park, Stanford, CA 94025, USA

[6]These authors contributed equally

[7]Lead Contact

*Correspondence: yicui@stanford.edu

https://doi.org/10.1016/j.joule.2019.01.017

Please cite this article in press as: Sun et al., Design of Red Phosphorus Nanostructured Electrode for Fast-Charging Lithium-Ion Batteries with High Energy Density, Joule (2019), https://doi.org/10.1016/j.joule.2019.01.017

stability windows. On the other hand, if the intrinsic potential of the anode is too close to 0 V (versus Li^+/Li), the large overpotentials involved during rapid charging may make the anode potential drop below 0 V (versus Li^+/Li) and prematurely terminate the electrochemical lithiation reactions, leading to low capacity retention. Even worse, Li metal plating takes place at such low potentials, giving rise to major safety concerns.[26,27] In other words, an ideal anode material for fast-charging LIBs should possess both high capacity and relatively low, yet safe, lithiation potential.

Here, we propose that red phosphorus (P) is an attractive anode material for fast-charging LIBs with high energy density due to the combined advantages of its high capacity and ideal lithiation potential. A red P-carbon (P/C) composite nanostructure, featuring micrometer-scale P/C composite grains with a conductive carbon superficial layer, a P/C composite core, internal nanometer-scale void space and red P nanodomain, and high density, has been successfully synthesized. The rationally designed P anode material delivers excellent fast-charging capability and high capacity based on the volume and weight of the whole electrode and presents the best cyclability and Coulombic efficiency (100.0% [$\pm$0.1%]) among all reported high-capacity anode materials at a commercial battery-level areal capacity.

RESULTS AND DISCUSSION

Anode Design for Fast-Charging LIBs

Figure 1B shows potential versus capacity plots for some typical anode materials. With its low lithiation potential (~0.1 V on average versus Li^+/Li) and limited capacity, graphite, the currently predominant anode, has inherent materials shortcomings for fast-charging LIBs. A commercial graphite electrode exhibits a high overpotential of ~0.12 V at 1 C and loses almost all its capacity in a half cell using an Li metal counter electrode due to this overpotential.[28] Although $Li_4Ti_5O_{12}$ has been widely studied[21,22] and is already used as an anode material for fast charging in electric buses, the energy density of LIBs with $Li_4Ti_5O_{12}$ anodes is severely limited by its high working potential (~1.5 V versus Li^+/Li) and low capacity (175 mAh g^{-1}, 611 mAh cm^{-3}). It is worthwhile to note that although Si displays the highest capacity among the electrode materials, its low lithiation potential (~0.2 V on average versus Li^+/Li) makes it non-ideal for fast-charging LIBs.[8] P reacts electrochemically with both Li and sodium via an alloy-reaction mechanism ($P + 3X^+ + 3e^- \rightarrow X_3P$, X: Li, Na) at an attractive potential (e.g., ~0.7 V in average versus Li^+/Li for red P) and delivers a high theoretical capacity (2,596 mAh g^{-1}, 6,075 mAh cm^{-3}).[29–34] Thus, P is an ideal anode material for fast-charging LIBs in consideration of both battery safety and energy density. Among the three main allotropes of P (white, red, and black),[35] red P is the most attractive because of its abundance, low cost, and good stability in air[36] and is suitable for widespread industrial applications.

Besides choosing the right materials, material structural design toward good electronic conductivity and space-efficient packing is also important for achieving good fast-charging capability. High conductivity and nanoscale structural design can facilitate fast electrochemical reactions and high active material utilization at the material level. Space-efficient packing of particles can reduce the thickness of electrodes and the electron and ion diffusion length at the electrode level, all while improving volumetric energy density of LIBs. In addition, in order to maintain a stable red P anode for fast-charging LIBs, close attention should be paid to addressing its tremendous volume change during the lithiation and delithiation process, which is a key challenge for all high-capacity battery chemistries.[37] Based on the analysis

Please cite this article in press as: Sun et al., Design of Red Phosphorus Nanostructured Electrode for Fast-Charging Lithium-Ion Batteries with High Energy Density, Joule (2019), https://doi.org/10.1016/j.joule.2019.01.017

above, the following points establish the guidelines for good structural design of red P anodes (Figure 1C): (1) good electronic conductivity at both the particle and electrode levels to facilitate fast electron transport,[37] (2) micrometer-scale particles and hierarchical particle size distribution to realize space-efficient packing,[38] and (3) internal nanoscale void space and red P nanodomain of particles to buffer the volume change and outer electrolyte blocking layer to stabilize the solid-electrolyte interface (SEI).[39]

Synthesis and Characterization of the P/C Nanocomposite

A simple, low-cost, large-scale (1 kg per batch) synthesis route was developed for the synthesis of a red P/C nanocomposite for fast-charging LIBs using an adsorption and surface cleaning strategy shown in Figure 2A. Micrometer-scale nanoporous carbon particles and red P powder were sealed in a stainless steel vessel in argon atmosphere and annealed at 450°C for 3 h. Above the sublimation temperature of red P (416°C), the produced P vapor penetrated into the nanoporous carbon particles and easily reached the inner nanopores. During the cooling process, the P vapor in the nanopores turned into red P that deposited onto the inner walls of the nanopores. These nanopores may not be fully filled, forming internal nanoscale void spaces since solid red P has higher density than P vapor. After cooling to room temperature, the superficial P on the P/C composite particles was cleaned away using solvent. An inexpensive, plant-derived porous carbon was chosen as the host for P filling because of its reasonable particle size (Figure S1), high specific surface area, and large pore volume (1,445 $m^2\ g^{-1}$ and 0.78 $cm^3\ g^{-1}$, respectively, by nitrogen sorption measurements; Figures 2B and S2). Transmission electron microscopy (TEM) images show that the carbon particles possess an interconnected nanoporous network with pore size less than 5 nm, in agreement with the nitrogen sorption results (Figures 2C and S2). These numerous nanopores with high porosity allow a high P filling content (~50 wt %), which enables high capacity based on the total weight and volume of the materials. The red P/C nanocomposite achieved by this process is stable for Li-ion batteries. The red P in porous carbon sublimes after 390°C under argon atmosphere (Figure S3A). Under air atmosphere, red P/porous carbon composite starts to catch fire at 480°C (Figure S3B), which is much higher than the temperature for thermal runaway of cells using conventional organic electrolyte (~180°C).[40]

Figure 2D shows a typical scanning transmission electron microscopy (STEM) and the corresponding energy-dispersive X-ray (EDX) elemental mapping images of the red P/C composite. The uniform elemental distribution of P and C in the whole investigated area is observed, suggesting that P is uniformly embedded into the carbon host. The specific surface area and pore volume of the P/C nanocomposite are only 9 $m^2\ g^{-1}$ and 0.02 $cm^3\ g^{-1}$ (Figures 2B and S2), respectively, indicating that almost all the nanopores of the particles are filled and/or blocked by red P. Figure 2E displays a representative high-resolution TEM (HRTEM) image for a P/C composite particle. In contrast to uniform grayscale of a pure porous carbon particle (Figure 2C), a dark-light contrast is clearly observed for a P/C composite particle, where the inner region is dark and the surface is light. The dark inner region of the particle is comprised of amorphous species and the nanopores of the carbon matrix cannot be observed, suggesting the embedding of amorphous red P nanodomains into the internal nanopores of the carbon. The amorphous structure of P is also confirmed by the X-ray diffraction (XRD) pattern, which shows no obvious peaks (Figure 2F). The amorphous structure and small size of red P nanodomains inside the nanopores of the carbon help to speed up the electrochemical reaction kinetics.[14] A light surface layer with thickness of ~20 nm is observed for

Please cite this article in press as: Sun et al., Design of Red Phosphorus Nanostructured Electrode for Fast-Charging Lithium-Ion Batteries with High Energy Density, Joule (2019), https://doi.org/10.1016/j.joule.2019.01.017

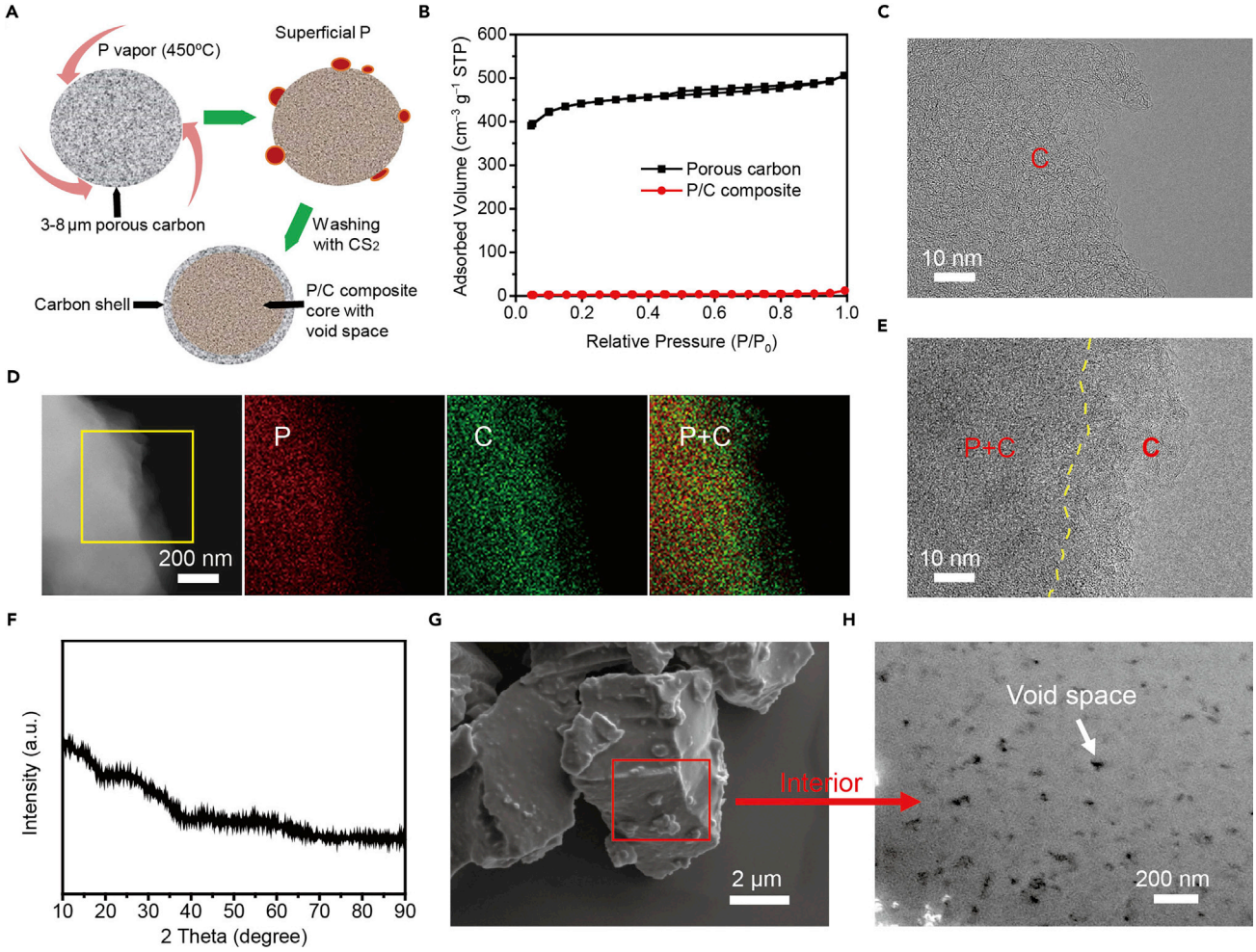

Figure 2. Synthesis and Characterization of the Red P/C Nanocomposite

(A) Schematic of the synthesis of the P/C nanocomposite. Micrometer-scale nanoporous carbon and red P powder are sealed in argon gas and annealed at 450°C so that P can transport into the nanopores of carbon via the diffusion of P vapor. P/C composite particles with a pure carbon nanolayer in the surface region and a P/C composite core with nanometer-scale void spaces and red P nanodomains in the inner region are achieved after the removal of the superficial red P.

(B) Nitrogen adsorption-desorption isotherms of the nanoporous carbon and the red P/C nanocomposite.

(C) HRTEM image of the nanoporous carbon.

(D–F) STEM and the corresponding EDX elemental mapping images (D), HRTEM image (E), and XRD pattern (F) of the P/C nanocomposite. The results indicate that amorphous red P is uniformly filled into the nanopores of the carbon host and the P on the surface of P/C composite particles is successfully removed away, forming a pure carbon superficial layer.

(G) SEM images of the red P/C nanocomposite.

(H) A cross-sectional SEM image of a red P/C composite particle showing the internal nanometer-scale void spaces. The cross section was realized by focused ion beam (FIB).

the same P/C composite particle, corresponding to a pure carbon surface (Figure 2E). Thus, the P/C composite particles possess a P-free thin carbon superficial layer and a P/C composite core with interior interconnected conductive network, which results in a high electrical conductivity of 2.3 S cm^{-1} for the P/C composite powders. The interior interconnected network of carbon creates a facile electron transport pathway within the P/C particles, and the pure carbon surface of such particles forms an electronically conductive network around and between neighboring particles to achieve good electrical conductivity at the electrode level, both of which are important in achieving fast electron transport at the materials

Please cite this article in press as: Sun et al., Design of Red Phosphorus Nanostructured Electrode for Fast-Charging Lithium-Ion Batteries with High Energy Density, Joule (2019), https://doi.org/10.1016/j.joule.2019.01.017

and electrode levels (Figure 1C). Moreover, the pure carbon surface prevents the direct contact between the P and electrolytes and limits side reactions.

Scanning electron microscopy (SEM) images show that the P/C nanocomposites have micrometer-scale particles with irregular shapes and a wide size distribution mainly between 3 to 8 μm (Figures 2G and S5), without obvious morphology changes in comparison with the bare carbon (Figure S1). The size and shape of the P/C nanocomposite particles promote space-efficient packing with a high- tap density of up to 1.0 g cm^{-3}, which facilitates the preparation of densely compacted electrodes with small thicknesses. A cross-sectional SEM image verifies the existence of numerous nanometer-scale void spaces inside the P/C composite particles (Figure 2H). These nanometer-scale void spaces can act as internal buffers for the local volume expansion of P and restrict the overall expansion of the whole P/C composite particles during the lithiation process, ensuring that the particles and electrodes remain intact upon long-term cycling, and the SEI on the particle surface is stable and thin.

Fast-Charging Capability of the P/C Electrode

The as-synthesized P/C composite nanostructure with high conductivity and short transport path for charge carriers affords remarkable fast-charging capability. Electrochemical measurements were performed at increasing cycling rates at a moderate areal capacity shown in Figures 3A and 3B. The initial 5 cycles were performed at slow rates of 0.1 and 0.2 *C*, allowing for the activation of materials and the formation of a stable SEI on the particle surface. The P/C electrode shows stable cycling over various current densities. It exhibits an average lithiation potential of 0.66 V versus Li^+/Li and a high specific capacity of 2,173 mAh g^{-1} at 1 *C*, corresponding to an areal capacity of 1.0 mAh cm^{-2} at 1.1 mA cm^{-2}. The specific capacity of the P/C electrode is as high as 1,829 mAh g^{-1} at 6 *C* (6.6 mA cm^{-2}). In other words, a battery with such a P/C anode can fill up 84% of its capacity within 10 min, reflecting its excellent fast-charging capability. Although a large overpotential of 0.36 V is produced at 8 *C* (8.8 mA cm^{-2}), the electrode shows a safe average lithiation potential of 0.30 V versus Li^+/Li and delivers a high specific capacity of 1,523 mAh g^{-1}, benefiting from the intrinsic, relatively high lithiation potential of red P and the optimized material structure design. To avoid the influence of the Li-metal counter electrode under a fast-charging rate in half cells during long-term cycling, $LiFePO_4$||P/C full cells were constructed. Charge and discharge measurements of the full cell using various charging rates and prolonged cycling at 4 *C* were performed (Figure S6). The capacity at 0.5 *C* (the 2^{nd} cycle) and 4 *C* were 124.0 mAh g^{-1} and 106.9 mAh g^{-1} (the 36^{th} cycle), respectively. Stable battery cycling was achieved at 4 *C* from the 36^{th} to 100^{th} cycles with high capacity retention of 96%.

Good fast-charging capability of electrodes at a high-areal capacity is of practical importance for industrial applications. To show the significant advantages of P/C electrodes for high energy density, fast-charging LIBs, P/C, $Li_4Ti_5O_{12}$ and graphite electrodes were closely compared with the same concentration (90 wt % materials, 5 wt % binder, and 5 wt % carbon black) and an industrial-level areal capacity of ~3.5 mAh cm^{-2} at 0.5 mA cm^{-2}. Figures 3C and 3D show the cross-section SEM images of P/C, $Li_4Ti_5O_{12}$ and graphite electrodes and their average thicknesses. Due to the high capacity of the P/C material and its space-efficient packing (Figure S7), the average thickness of P/C electrodes is 21.5 μm, much thinner than the 76.3 and 124.5 μm for $Li_4Ti_5O_{12}$ and graphite electrodes, respectively (Figure 3D; Table S1). The much smaller thickness of the P/C electrodes provides a much shorter path to facilitate fast ion and electron transport at the electrode level. Meanwhile, a

Please cite this article in press as: Sun et al., Design of Red Phosphorus Nanostructured Electrode for Fast-Charging Lithium-Ion Batteries with High Energy Density, Joule (2019), https://doi.org/10.1016/j.joule.2019.01.017

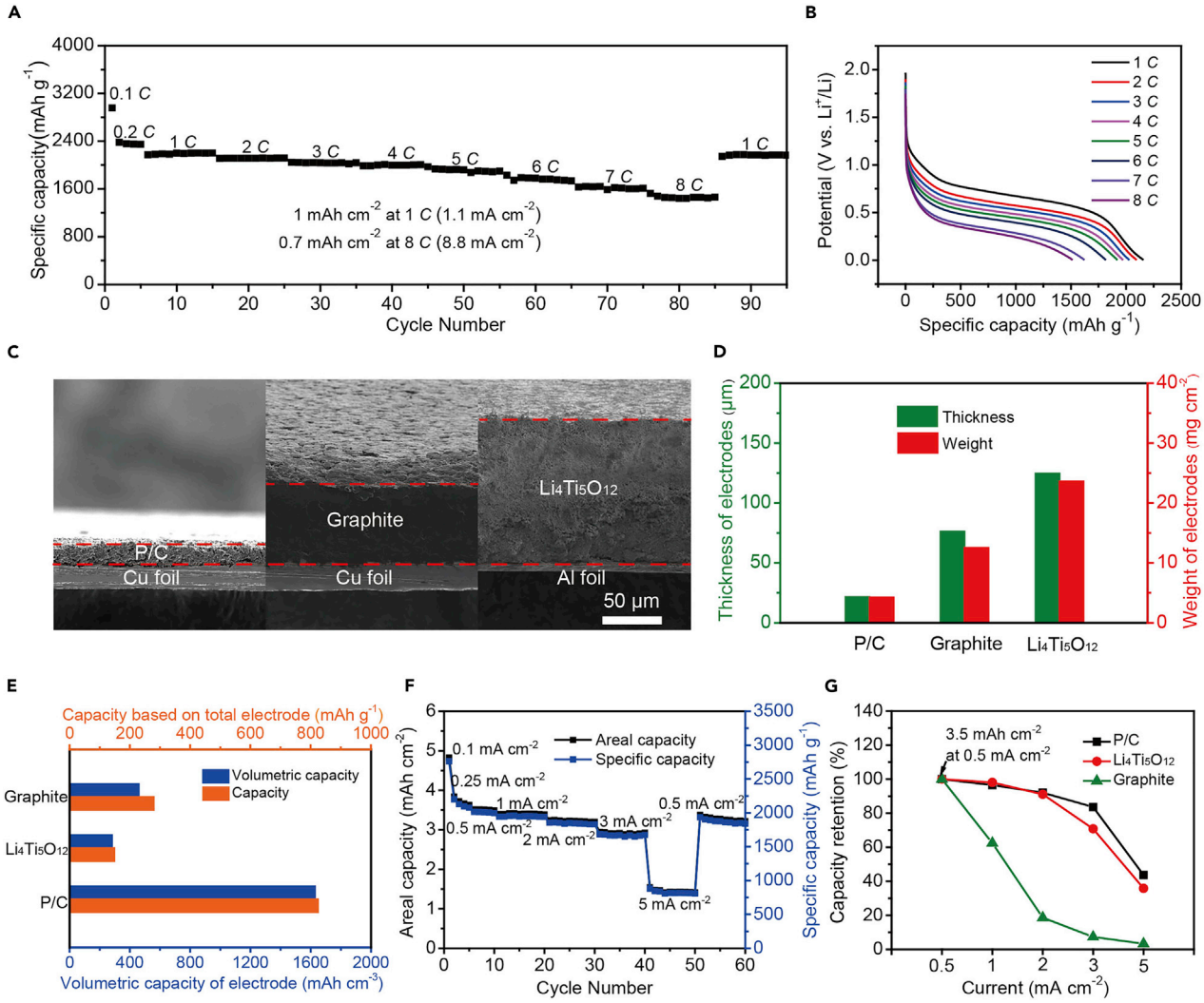

Figure 3. Rate Capability of P/C Electrodes

(A and B) A P/C electrode with an areal capacity of 1 mAh cm^{-2} (at 1 *C*, 1.1 mA cm^{-2}) cycled from 1 to 8 *C* after 5 activation cycles at 0.1 and 0.2 *C* (A), and the corresponding potential profiles during the lithiation processes (B). The average lithiation potential of the P/C electrode is ~0.3 V versus Li^+/Li at 8 C, which is high enough to release the capacity and avoid lithium metal plating.

(C–E) Cross-section SEM images (C), the comparison of the thicknesses and weights (D), and capacities and volumetric capacities based on the total electrode (active material, binder, and carbon) for P/C, graphite, and $Li_4Ti_5O_{12}$ electrodes with the same areal capacity (~3.5 mAh cm^{-2} at 0.5 mA cm^{-2}) (E).

(F) A P/C electrode with an areal capacity of ~3.5 mAh cm^{-2} at 0.5 mA cm^{-2} cycled at various areal current densities.

(G) Comparison of capacity retentions for P/C, commercial $Li_4Ti_5O_{12}$, and graphite electrodes with the same areal capacity of ~3.5 mAh cm^{-2} at 0.5 mA cm^{-2}. All the electrodes comprise 90 wt % materials, 5 wt % binder, and 5 wt % carbon black.

high volumetric capacity of 1,628 mAh cm^{-3} is achieved based on the whole P/C electrode, which is significantly higher than that of $Li_4Ti_5O_{12}$ and graphite electrodes (459 and 281 mAh cm^{-3}, respectively) (Figure 3E). Moreover, the P/C electrode delivers the highest capacity based on the total weight of the electrodes. The average total weight of the P/C electrode is 4.3 mg cm^{-2}, which is much less than 12.5 mg cm^{-2} for the graphite electrode and 23.6 mg cm^{-2} for the $Li_4Ti_5O_{12}$ electrode (Figure 3D; Table S1). The capacities based on the average total weight of electrodes are 824, 148, and 279 mAh g^{-1} for the P/C, $Li_4Ti_5O_{12}$ and graphite, respectively (Figure 3E; Table S1). To better evaluate the capacity of battery electrodes, one should normalize the capacity based on the total weight of electrode,

Please cite this article in press as: Sun et al., Design of Red Phosphorus Nanostructured Electrode for Fast-Charging Lithium-Ion Batteries with High Energy Density, Joule (2019), https://doi.org/10.1016/j.joule.2019.01.017

current collector, and electrolyte intake.[41] The data were collected and analyzed in Table. S2. Due to the small electrode thickness and weight, the electrolyte intake for the P/C electrode (0.25 mg cm^{-2}) is much less than that for $Li_4Ti_5O_{12}$ (9.08 mg cm^{-2}) and graphite (4.03 mg cm^{-2}) electrodes. The total weight of the P/C electrode, including electrode, absorbed electrolyte, and current collector, is 11.70 mg cm^{-2}, much less than the 35.66 mg cm^{-2} for the $Li_4Ti_5O_{12}$ electrode and the 23.76 mg cm^{-2} for the graphite electrode, even when considering that the weight and density of the Cu current collector for the P/C electrode is higher than that of the Al current collector for the $Li_4Ti_5O_{12}$ electrode. Normalized for the total weight, the capacity of the P/C electrode is 299 mAh g^{-1}, which is much higher than 98 mAh g^{-1} for $Li_4Ti_5O_{12}$ electrode and 147 mAh g^{-1} for graphite electrode. Additionally, beyond just the much higher capacity of the P/C anode than the $Li_4Ti_5O_{12}$ electrode, the P/C electrode exhibits much lower working potential (~0.7 V) than the $Li_4Ti_5O_{12}$ electrode (~1.5 V). Much higher energy density can thus be achieved for the cells using the P/C anode than the $Li_4Ti_5O_{12}$ anode. Therefore, by using such high-capacity P/C electrodes with small thickness, high-energy-density LIBs with excellent fast-charging capability can be realized.

Charging capability of these P/C, graphite, and $Li_4Ti_5O_{12}$ electrodes was measured by changing the lithiation current density from 0.25 to 5 mA cm^{-2}. As shown in Figure 3F, the areal capacity of the tested P/C electrode is 3.52 mAh cm^{-2} at 0.5 mA cm^{-2}, corresponding to a high specific capacity of 2,015 mAh g^{-1}. When the current density is increased from 0.5 to 3 mA cm^{-2}, only a slight decrease in capacity is observed. The P/C electrode delivers an areal capacity of 2.94 mAh cm^{-2} at 3 mA cm^{-2}, corresponding to a high specific capacity of 1,684 mAh g^{-1}. Meanwhile, an areal capacity of 1.54 mAh cm^{-2} is achieved at a high-areal current density of 5 mA cm^{-2}. The rate-dependent charging capability of graphite and $Li_4Ti_5O_{12}$ electrodes were also measured (Figures S8 and S9). Figure 3G compares the capacity retention for the P/C, $Li_4Ti_5O_{12}$ and graphite electrodes at various areal current densities. The graphite electrode loses most of its capacity at 2 mA cm^{-2}. In contrast, the $Li_4Ti_5O_{12}$ has 91% capacity retention at 2 mA cm^{-2}, showing much better rate capability. Impressively, the P/C electrode has capacity retention (92%) comparable to that of $Li_4Ti_5O_{12}$ at 2 mA cm^{-2} and even higher capacity retention at higher current densities. The P/C electrode retains 84%% and 44% of its capacity at 3 and 5 mA cm^{-2}, respectively, much higher than the 71% and 36% for the $Li_4Ti_5O_{12}$ electrode, demonstrating the superior fast-charging capability of the P/C electrode at an areal capacity level of a commercial Li-ion battery cell.

Cycling Stability of the P/C Electrode

The P/C nanocomposite also affords remarkable cycle life at the areal capacity level of a commercial Li-ion battery cell (Figure 4A). For a good comparison with previous reports,[29,30,36] the content of P/C material in the electrode was 80 wt %. A P/C electrode with 1.6 mg cm^{-2} P loading delivers a discharge areal capacity of 3.0 mAh cm^{-2} at the 10^{th} cycle at 0.86 mA cm^{-2} (*C*/5) and 90% capacity retention at the 500^{th} cycle. The corresponding discharge-specific capacity for the 500^{th} cycle is 1,625 mAh g^{-1}, which is more than 4 and 9 times the theoretical capacities of graphite and $Li_4Ti_5O_{12}$, respectively. This is the first time that both appropriately high-areal capacity and stable long-term cycling have been shown for P-based anodes, and the cycle stability is among the best for high-capacity anodes.[42] This remarkable cycling performance data should be distinguished from most commonly reported results (Table S3), which are normalized by the weight of active materials at a low-areal capacity or shown with limited cycles (e.g., 100 or less cycles). The P/C electrode exhibits stable sloping lithiation and delithiation

Please cite this article in press as: Sun et al., Design of Red Phosphorus Nanostructured Electrode for Fast-Charging Lithium-Ion Batteries with High Energy Density, Joule (2019), https://doi.org/10.1016/j.joule.2019.01.017

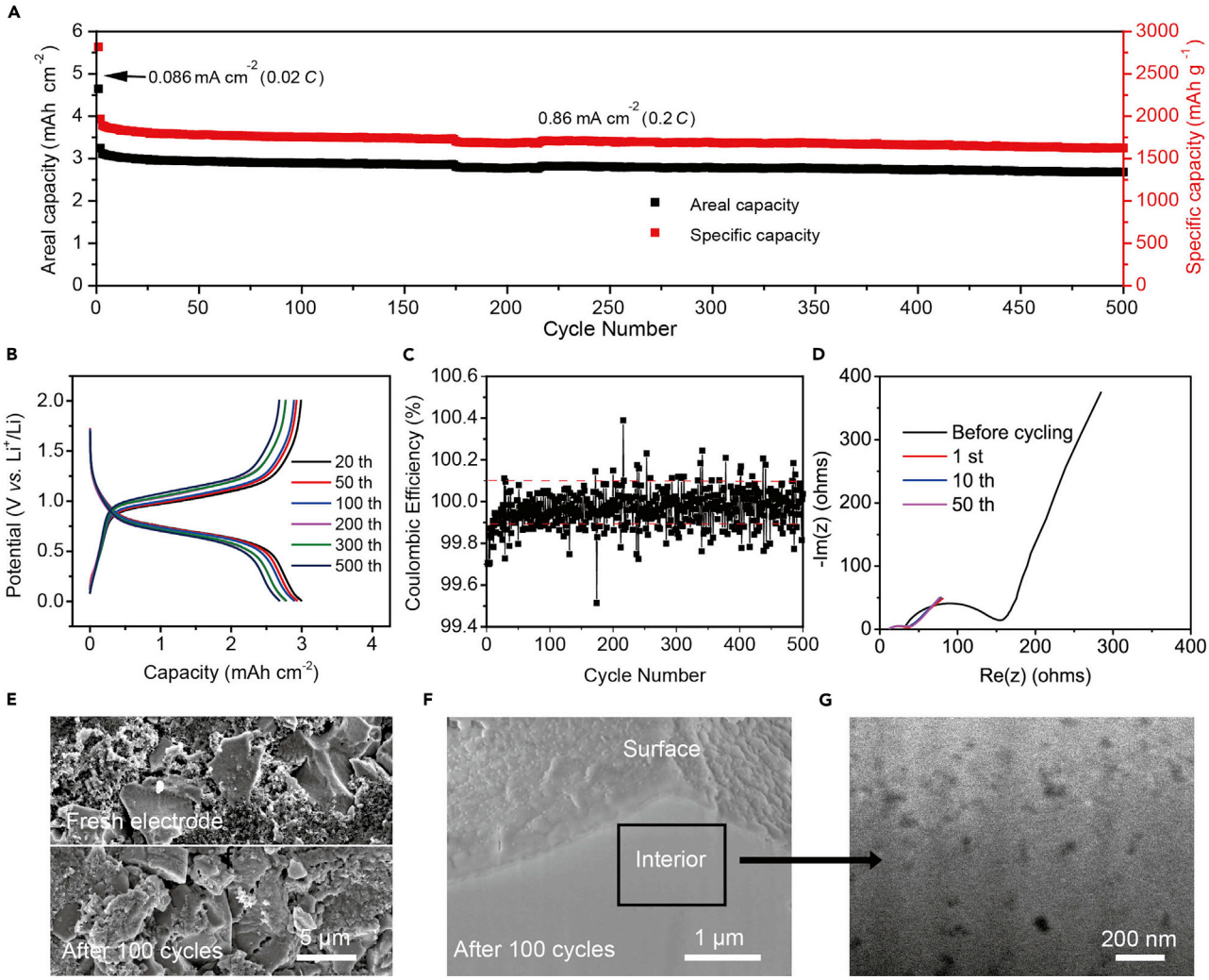

Figure 4. Cycling Stability of P/C Electrodes

(A–C) Discharge areal and specific capacity versus cycle number of a P/C electrode for 500 cycles (A), the corresponding potential profiles for various cycles (B), and Coulombic efficiencies during cycling (C). The mass loading of P is 1.6 mg cm^{-2}. The current densities are 0.086 mA cm^{-2} (0.02 *C*) for the first cycle and 0.86 mA cm^{-2} (0.2 *C*) for the following cycles. The specific capacity here is calculated based on the mass of P.

(D) Electrochemical impedance spectra of a P/C electrode after different discharge-charge cycles over the frequency range from 100 kHz to 0.1 Hz.

(E) Top-view SEM images of P/C electrodes before and after 100 cycles at *C*/5, showing no cleavages or cracks at the particle level.

(F and G) Cross-section SEM images of a P/C composite particle after 100 cycles (F) with interior box enlarged (G). The cross section was realized by FIB.

potential profiles with an average lithiation voltage of 0.69 V (versus Li^+/Li), delithiation voltage of 1.02 V (versus Li^+/Li), and potential hysteresis of 0.33 V during cycling (Figure 4B). Only a slight increase in overpotential and decrease in capacity are observed after 500 cycles, which may arise from the degradation of the Li-metal counter electrode.

In addition to capacity stability, Coulombic efficiency is another important concern for high-capacity electrode materials. The initial-cycle Coulombic efficiency of the P/C electrode corresponding to Figure 4A is 80.5% (Figure S10). This initial loss of Li can be addressed by prelithiation strategies in a full-cell configuration.[43] The Coulombic efficiency exhibits a rapid increase during cycling, reaching 96.1%,

99.7%, and 99.8% for the 2nd, 3rd, and 4th cycle, respectively, and it is maintained at high values between 99.9% and 100.1% after the 4th cycle, with an average Coulombic efficiency of 100.0% (Figure 4C), which is similar to, if not better than, the commercial graphite anode. Stable and high Coulombic efficiency is a decisive factor for the practical application of high-capacity anode materials into full-cell systems, and therefore, in this respect, our results indicate great promise for the industrial application of P/C electrodes. The Nyquist plots of the as-prepared P/C electrodes show a suppressed semicircle in the high-middle-frequency region and an oblique straight line in the low-frequency region for different cycles (Figure 4D). The semicircle diameter of the plot for the first cycle is much larger than that for the following cycles, mainly due to the reduced contact or interfacial impedance of the electrolyte against the Li-metal counter electrode after the first cycle. The similar semicircle diameters after the first cycle verify the good stability of the P/C electrodes.

Stable cycling of a high-areal-capacity electrode with excellent Coulombic efficiencies has strict requirements in terms of structural stability both at the particle and electrode levels. SEM imaging was performed to investigate and compare the morphology and structure of the P/C nanocomposite and electrode before and after 100 cycles. The cycled electrode remains in good contact with the current collector (Figure S11) and preserves its morphological integrity and electrical interconnectivity throughout the whole measured area without any cracks and contact losses (Figures 4E and S12). Meanwhile, no cracks are observed for individual P/C composite particles after cycling (Figure S13). To more closely investigate the structural stability of the P/C nanocomposite at the particle level, an *in situ* electrochemical cell was built inside the TEM (Figure S14; Videos S1 and S2). In contrast to the large volume expansion of pure P (~300%), only a slight volume expansion (~12% in one dimension, ~40% for the whole particle) was observed during the lithiation process of one single P/C composite particle, and the investigated particle preserved its structural integrity throughout the lithiation and delithiation processes without any cracking. The volume expansion at the particle level in the *in situ* TEM experiment should be different from the electrode-based volume change or thickness variation during cycling. The interspace between particles in the electrode may accommodate some volume change of the particles during the lithiation and delithiation processes. Thus, it is expected that the measured volume expansion at the electrode level will be smaller than that of a single particle observed using the *in situ* TEM. A Vernier caliper provides direct and accurate measurement of the thickness of electrodes. The volume change of the overall electrode during charging and discharging depending on time was investigated. The value of the thickness change of a P/C electrode is reversible after the first cycle. The thickness was 72 μm for the fully charged state and 58 μm for the fully discharged state for a P/C electrode with an areal capacity of ~3.5 mAh cm^{-2} at 0.5 mAh cm^{-2} after the first cycle. The corresponding reversible electrode expansion in the thickness of the electrode is ~25%. Cross-section SEM images of a P/C composite particle show that a uniform and thin SEI layer (< 50 nm) forms on the outer surface of a P/C composite particle (Figure 4F) after 100 cycles and the interior nanoscale void spaces are well maintained for buffering volume change (Figure 4G). These results indicate that good structural stability of the P/C composite is maintained both at the electrode and at the particle level, which enables stable battery cycling and high a Coulombic efficiency of 100.0%. Moreover, defects in the activated carbon produced from coconut shell may also have advantages in improving the cycling stability of the as-achieved P/C anode.[44]

Please cite this article in press as: Sun et al., Design of Red Phosphorus Nanostructured Electrode for Fast-Charging Lithium-Ion Batteries with High Energy Density, Joule (2019), https://doi.org/10.1016/j.joule.2019.01.017

Conclusions

Our studies show that red P with high capacity and relatively low, yet safe, lithiation potential is an attractive anode material for high energy density, fast-charging LIBs. We demonstrate that electrodes utilizing a red P/C nanocomposite with an optimized structure display much better capacity retention and deliver a much higher capacity based on both the total weight and volume of the electrodes than that of the commercial graphite and $Li_4Ti_5O_{12}$ electrodes at the areal-capacity level of a commercial Li-ion battery cell (~3.5 mAh cm^{-2}). Furthermore, the P/C electrode displays a combination of stable cycling and 100.0% (±0.1%) Coulombic efficiency during cycling at an appropriately high-areal capacity of ~3 mAh cm^{-2}. Due to its superior electrochemical performance, easy preparation, and low cost, we believe that the P/C nanocomposite will have important applications in advanced fast-charging LIBs with high energy density.

EXPERIMENTAL PROCEDURES

Materials Synthesis

Coconut-shell-derived, hierarchically nanoporous carbon particles were prepared according to a previous report with minor modifications.[45] Coconut shells were first cleaned, crushed, and sieved. The coconut shells were carbonized under nitrogen atmosphere at 700°C for 2 h. The as-achieved carbon was then soaked in 50 wt % potassium hydroxide (KOH) solution with KOH/C mass ratio of 4. After drying at 120°C for 5 h, the mixture was heated to 850°C under nitrogen gas flow and followed by activation for 2 h under carbon dioxide (CO_2) gas flow. Porous carbon was achieved after washing. The red P/C nanocomposite was prepared using a vaporization, adsorption, and surface cleaning method.[46–49] Commercial red P and the as-achieved nanoporous carbon particles with micrometer size were used as the starting materials. Red P was milled and washed with deionized water before using. Porous carbon particles and excess red P powder were sealed in a stainless-steel vessel in argon atmosphere and annealed at 450°C for 3 h. The excess red P makes sure that there is enough P vapor and pressure for the conversion from white P to red P and the long cooling time of 15 h provides enough time for this conversion. Last, the superficial P on the P/C composite particles was washed away using CS_2 solvent to form a pure carbon surface. The washing process was performed in the hood to avoid the intake of toxic CS_2 vapor. For future application in industrial battery materials synthesis and battery manufacturing, there are documented safety measures for the use of toxic solvents (e.g., CS_2).

Characterizations

The SEM images were taken with an FEI XL30 Sirion SEM. An FEI Helios NanoLab 600i DualBeam FIB/SEM system was used to acquire the cross-section SEM images of the P/C particles. The XRD measurements were conducted on a panalytical X'pert diffractometer with Ni-filtered Cu Kα radiation. The thicknesses of electrodes were measured using a Vernier caliper. An FEI Titan 80–300 environmental TEM was used for TEM, high-resolution TEM (HRTEM), and STEM images; energy-dispersive X-ray spectroscopy (EDS) mapping and electron energy loss spectroscopy (EELS) spectra collection; and *in situ* TEM measurements. The *in situ* electrochemical cell was built in a piezo-controlled, electrical biasing TEM-AFM (atomic force microscopy) holder (Nanofactory Instruments) with a P/C particle as the working electrode and Li metal as the counter electrode. By applying a voltage bias, Li ions flowed through the native oxide layer of Li metal to react with P reversibly. A standard four-probe method was used for the electrical conductivity measurement of the red P/C nanocomposite. Before measurement, the sample powders were compressed into a pellet of 10 mm in diameter and 1 mm in thickness under a pressure of 20 MPa.

Electrochemical Measurements

A slurry method was used to prepare the electrodes by mixing the active materials, carbon black, and polyvinylidene fluoride (PVDF) binder in N-methyl-2-pyrrolidinone (NMP) solvent. The electrodes (P/C, $Li_4Ti_5O_{12}$, and graphite) for rate capability measurements were prepared with 90 wt % materials, 5 wt % carbon black, and 5 wt % PVDF binder. P/C electrodes with two different total mass loadings of 0.9–1.1 mg cm^{-2} and 4.2–4.4 mg cm^{-2} are used in our experiment. The corresponding mass loadings of active P are 0.4–0.5 mg cm^{-2} and 1.9–2.0 mg cm^{-2}, respectively. P/C electrodes were tested for long-term cycling stability with 80 wt % of P/C composite, 10 wt % carbon black, and 10 wt % PVDF, with a P mass loading of 1.6–1.7 mg cm^{-2}, and total mass loading of 4.0–4.2 mg cm^{-2}. 2032-type coin cell (MTI Corporation) cells were assembled in an Argon-filled glove box using Li metal as the counter electrode, a Celgard 2325 membrane as the separator, and 1-M $LiPF_6$ in a mixture of ethylene carbonate (EC) and diethyl carbonate (DEC) (1:1 v/v) as the electrolyte. 120 μL of electrolyte was used for the coin-cell configuration. The battery performances were recorded on an Arbin 96-channel battery tester or a LAND 8-channel battery tester. The galvanostatic charge and discharge measurement for P/C||Li-metal cells was carried out with the cut-off potential range of 0.01–2 V. Graphite||Li-metal cells were charged and discharged between 0.01 and 1 V. The cut-off potential range for $Li_4Ti_5O_{12}$/Li-metal cells was 1–2.5 V. For the measurement of fast-charging capability of our P/C anode, half cells using Li metal as the counter electrode were assembled. To minimize the influence from the Li-metal counter electrode, P/C||Li-metal cells were discharged at increasing *C* rate but charged at constant *C*/5 rate. The values of the overpotential at fast-charging rates were calculated by taking the potential difference between potential plateau at fast rates and the equilibrium potentials calculated according to the charge-discharge curves at a low current rate of 0.2 *C*. The specific capacity is calculated based on the mass of P, if not stated otherwise.

SUPPLEMENTAL INFORMATION

Supplemental Information can be found with this article online at https://doi.org/10.1016/j.joule.2019.01.017.

ACKNOWLEDGMENTS

Y.C. acknowledges support from the Assistant Secretary for Energy Efficiency and Renewable Energy, Office of Vehicle Technologies of the U.S. Department of Energy under the Extreme Fast Charging (XFC) program.

AUTHOR CONTRIBUTIONS

Y.S., L.W., X.H., and Y.C. conceived the concept and experiments. Y.S. and L.W. performed materials characterization and electrochemical measurements with assistance from Yanbin Li, Yuzhang Li, and H.R.L. A.P., Y.S., L.W., and Y.C. co-wrote the paper. All authors discussed the results and commented on the manuscript.

DECLARATION OF INTERESTS

The authors declare no competing interests.

Received: October 12, 2018
Revised: December 2, 2018
Accepted: January 25, 2019
Published: March 6, 2019

REFERENCES

1. Armand, M., and Tarascon, J.M. (2008). Building better batteries. Nature *451*, 652–657.
2. Chu, S., Cui, Y., and Liu, N. (2016). The path towards sustainable energy. Nat. Mater. *16*, 16–22.
3. Dunn, B., Kamath, H., and Tarascon, J.M. (2011). Electrical energy storage for the grid: A battery of choices. Science *334*, 928–935.
4. Choi, N.S., Chen, Z., Freunberger, S.A., Ji, X., Sun, Y.K., Amine, K., Yushin, G., Nazar, L.F., Cho, J., and Bruce, P.G. (2012). Challenges facing lithium batteries and electrical double-layer capacitors. Angew. Chem. Int. Ed. *51*, 9994–10024.
5. Goodenough, J.B. (2013). Evolution of strategies for modern rechargeable batteries. Acc. Chem. Res. *46*, 1053–1061.
6. Thackeray, M.M., Wolverton, C., and Isaacs, E.D. (2012). Electrical energy storage for transportation-approaching the limits of, and going beyond, lithium-ion batteries. Energy Environ. Sci. *5*, 7854–7863.
7. Scrosati, B., and Garche, J. (2010). Lithium batteries: status, prospects and future. J. Power Sources *195*, 2419–2430.
8. Chan, C.K., Peng, H., Liu, G., McIlwrath, K., Zhang, X.F., Huggins, R.A., and Cui, Y. (2008). High-performance lithium battery anodes using silicon nanowires. Nat. Nanotechnol. *3*, 31–35.
9. Kovalenko, I., Zdyrko, B., Magasinski, A., Hertzberg, B., Milicev, Z., Burtovyy, R., Luzinov, I., and Yushin, G. (2011). A major constituent of brown algae for use in high-capacity Li-ion batteries. Science *334*, 75–79.
10. Luo, Z., Xiao, Q., Lei, G., Li, Z., and Tang, C. (2016). Si nanoparticles/graphene composite membrane for high performance silicon anode in lithium ion batteries. Carbon *98*, 373–380.
11. Lin, D., Liu, Y., and Cui, Y. (2017). Reviving the lithium metal anode for high-energy batteries. Nat. Nanotechnol. *12*, 194–206.
12. Varzi, A., Raccichini, R., Passerini, S., and Scrosati, B. (2016). Challenges and prospects of the role of solid electrolytes in the revitalization of lithium metal batteries. J. Mater. Chem. A *4*, 17251–17259.
13. Seh, Z.W., Sun, Y., Zhang, Q., and Cui, Y. (2016). Designing high-energy lithium-sulfur batteries. Chem. Soc. Rev. *45*, 5605–5634.
14. Ji, X.L., Lee, K.T., and Nazar, L.F. (2009). A highly ordered nanostructured carbon-sulphur cathode for lithium-sulphur batteries. Nat. Mater. *8*, 500–506.
15. Agostini, M., Scrosati, B., and Hassoun, J. (2015). An advanced lithium-ion sulfur battery for high energy storage. Adv. Energy Mater. *5*, 1500481.
16. Peng, H.J., Huang, J.Q., Liu, X.Y., Cheng, X.B., Xu, W.T., Zhao, C.Z., Wei, F., and Zhang, Q. (2017). Healing high-loading sulfur electrodes with unprecedented long cycling life: Spatial heterogeneity control. J. Am. Chem. Soc. *139*, 8458–8466.
17. Bruce, P.G., Freunberger, S.A., Hardwick, L.J., and Tarascon, J.M. (2011). Li-O_2 and Li-S batteries with high energy storage. Nat. Mater. *11*, 19–29.
18. Lu, J., Lee, Y.J., Luo, X., Lau, K.C., Asadi, M., Wang, H.H., Brombosz, S., Wen, J., Zhai, D., Chen, Z., et al. (2016). A lithium–oxygen battery based on lithium superoxide. Nature *529*, 377–382.
19. Sun, Y.K., and Yoon, C.S. (2017). Lithium–oxygen batteries: the reaction mechanism revealed. Nat. Nanotechnol. *12*, 503–504.
20. Tang, Y., Zhang, Y., Li, W., Ma, B., and Chen, X. (2015). Rational material design for ultrafast rechargeable lithium-ion batteries. Chem. Soc. Rev. *44*, 5926–5940.
21. Jung, H.G., Jang, M.W., Hassoun, J., Sun, Y.K., and Scrosati, B. (2011). A high-rate long-life $Li_4Ti_5O_{12}$/$Li[Ni_{0.45}Co_{0.1}Mn_{1.45}]O_4$ lithium-ion battery. Nat. Commun. *2*, 516.
22. Wang, Y.Q., Gu, L., Guo, Y.G., Li, H., He, X.Q., Tsukimoto, S., Ikuhara, Y., and Wan, L.J. (2012). Rutile-TiO_2 nanocoating for a high-rate $Li_4Ti_5O_{12}$ anode of a lithium-ion battery. J. Am. Chem. Soc. *134*, 7874–7879.
23. Yuan, L.-X., Wang, Z.-H., Zhang, W.-X., Hu, X.-L., Chen, J.-T., Huang, Y.-H., and Goodenough, J.B. (2011). Development and challenges of $LiFePO_4$ cathode material for lithium-ion batteries. Energy Environ. Sci. *4*, 269–284.
24. Sun, H., Mei, L., Liang, J., Zhao, Z., Lee, C., Fei, H., Ding, M., Lau, J., Li, M., Wang, C., et al. (2017). Three-dimensional holey-graphene/niobia composite architectures for ultrahigh-rate energy storage. Science *356*, 599–604.
25. Shen, L., Chen, S., Maier, J., and Yu, Y. (2017). Carbon-coated Li_3VO_4 spheres as constituents of an advanced anode material for high-rate long-life lithium-ion batteries. Adv. Mater. *29*, 1701571.
26. Uhlmann, C., Illig, J., Ender, M., Schuster, R., and Ivers-Tiffée, E. (2015). In situ detection of lithium metal plating on graphite in experimental cells. J. Power Sources *279*, 428–438.
27. Park, C.-K., Zhang, Z., Xu, Z., Kakirde, A., Kang, K., Chai, C., Au, G., and Cristo, L. (2007). Variables study for the fast charging lithium ion batteries. J. Power Sources *165*, 892–896.
28. Billaud, J., Bouville, F., Magrini, T., Villevieille, C., and Studart, A.R. (2016). Magnetically aligned graphite electrodes for high-rate performance Li-ion batteries. Nat. Energy *1*, 16097.
29. Marino, C., Debenedetti, A., Fraisse, B., Favier, F., and Monconduit, L. (2011). Activated-phosphorus as new electrode material for Li-ion batteries. Electrochem. Commun. *13*, 346–349.
30. Qian, J., Qiao, D., Ai, X., Cao, Y., and Yang, H. (2012). Reversible 3-Li storage reactions of amorphous phosphorus as high capacity and cycling-stable anodes for Li-ion batteries. Chem. Commun. (Camb.) *48*, 8931–8933.
31. Sun, J., Lee, H.W., Pasta, M., Yuan, H., Zheng, G., Sun, Y., Li, Y., and Cui, Y. (2015). A phosphorene–graphene hybrid material as a high-capacity anode for sodium-ion batteries. Nat. Nanotechnol. *10*, 980–985.
32. Sun, J., Zheng, G., Lee, H.W., Liu, N., Wang, H., Yao, H., Yang, W., and Cui, Y. (2014). Formation of stable phosphorus–carbon bond for enhanced performance in black phosphorus nanoparticle–graphite composite nattery anodes. Nano Lett. *14*, 4573–4580.
33. Li, W., Yang, Z., Jiang, Y., Yu, Z., Gu, L., and Yu, Y. (2014). Crystalline red phosphorus incorporated with porous carbon nanofibers as flexible electrode for high performance lithium-ion batteries. Carbon *78*, 455–462.
34. Yue, Z., Gupta, T., Wang, F., Li, C., Kumar, R., Yang, Z., and Koratkar, N. (2018). Utilizing a graphene matrix to overcome the intrinsic limitations of red phosphorus as an anode material in lithium-ion batteries. Carbon *127*, 588–595.
35. Corbridge, D.E.C. (2013). Phosphorus Chemistry, Biochemistry and Technology 6th edn (CRC Press).
36. Wang, L., He, X., Li, J., Sun, W., Gao, J., Guo, J., and Jiang, C. (2012). Nano-structured phosphorus composite as high-capacity anode materials for lithium batteries. Angew. Chem. Int. Ed. *51*, 9034–9037.
37. Sun, Y., Liu, N., and Cui, Y. (2016). Promises and challenges of nanomaterials for lithium-based rechargeable batteries. Nat. Energy *1*, 16071.
38. Liu, N., Lu, Z., Zhao, J., McDowell, M.T., Lee, H.W., Zhao, W., and Cui, Y. (2014). A pomegranate-inspired nanoscale design for large-volume-change lithium battery anodes. Nat. Nanotechnol. *9*, 187–192.
39. Wu, H., Chan, G., Choi, J.W., Ryu, I., Yao, Y., McDowell, M.T., Lee, S.W., Jackson, A., Yang, Y., Hu, L., et al. (2012). Stable cycling of double-walled silicon nanotube battery anodes through solid-electrolyte interphase control. Nat. Nanotechnol. *7*, 310–315.
40. Abraham, D.P., Roth, E.P., Kostecki, R., McCarthy, K., MacLaren, S., and Doughty, D.H. (2006). Diagnostic examination of thermally abused high-power lithium-ion cells. J. Power Sources *161*, 648–657.
41. McCloskey, B.D. (2015). Attainable gravimetric and volumetric energy density of Li–S and Li ion battery cells with solid separator-protected Li metal anodes. J. Phys. Chem. Lett. *6*, 4581–4588.
42. Aravindan, V., Lee, Y.-S., and Madhavi, S. (2015). Research progress on negative electrodes for practical Li-ion batteries: Beyond carbonaceous anodes. Adv. Energy Mater. *5*, 1402225.
43. Aravindan, V., Lee, Y.-S., and Madhavi, S. (2017). Best Practices for mitigating irreversible capacity loss of negative electrodes in Li-ion batteries. Adv. Energy Mater. *7*, 1602607.
44. Li, M., Carter, R., Oakes, L., Douglas, A., Muralidharan, N., and Pint, C.L. (2017). Role of carbon defects in the reversible alloying states

of red phosphorus composite anodes for efficient sodium ion batteries. J. Mater. Chem. A *5*, 5266–5272.

45. Tan, I.A.W., Ahmad, A.L., and Hameed, B.H.J. (2008). Adsorption of basic dye on high-surface-area activated carbon prepared from coconut husk: Equilibrium, kinetic and thermodynamic studies. J. Hazard. Mater. *154*, 337–346.

46. Li, J., Qian, Y., Wang, L., and He, X. (2018). Nitrogen-doped carbon for red phosphorous based anode materials for lithium ion batteries. Materials (Basel) *11*, 134.

47. Yu, Z., Song, J., Wang, D., and Wang, D. (2017). Advanced anode for sodium-ion battery with promising long cycling stability achieved by tuning phosphorus-carbon nanostructures. Nano Energy *40*, 550–558.

48. Li, W., Hu, S., Luo, X., Li, Z., Sun, X., Li, M., Liu, F., and Yu, Y. (2017). Confined amorphous red phosphorus in MOF-derived N-doped microporous carbon as a superior anode for sodium-ion battery. Adv. Mater. *29*, 1605820.

49. Li, J., Wang, L., Wang, Z., Tian, G., and He, X. (2017). Economic and high performance phosphorus-carbon composite for lithium and sodium storage. ACS Omega *2*, 4440–4446.